JPET Fast Forward. Published on April 11, 2018 as DOI: 10.1124/jpet.118.247767
This article has not been copyedited and formatted. The final version may differ from this version.

Title page

In vitro – *in vivo* extrapolation of OATP1B-mediated drug-drug interactions in cynomolgus monkey

A. Ufuk, R. E. Kosa, H. Gao, YA. Bi, S. Modi, D. Gates, A. D. Rodrigues, L. M. Tremaine , M. V. S. Varma, J. B. Houston and A. Galetin

Centre for Applied Pharmacokinetic Research, School of Medicine, Biology and Health Sciences, University of Manchester, UK (AU, JBH and AG)

Pharmacokinetics, Dynamics and Metabolism, Medicine Design, Pfizer Worldwide R&D, Groton, CT (REK, HG, YAB, ADR, LMT and MVSV)

Research Formulations, Pharmaceutical Sciences, Medicine Design, Pfizer Worldwide R&D, Groton, CT (SM and DG)

Running title page

Running title: IVIVE of OATP DDIs in cynomolgus monkey

Corresponding Author: Dr Aleksandra Galetin

Centre for Applied Pharmacokinetic Research

School of Health Sciences,

University of Manchester,

Stopford Building, Oxford Road, Manchester, M13 9PT, UK

Tel: (+) 44 161 275 6886

Email: Aleksandra.Galetin@manchester.ac.uk

Topic Category: Metabolism, Transport and Pharmacogenomics

Number of text pages: 32

Number of tables: 3

Number of Figures: 7

Number of references: 45

Number of words in Abstract: 249

Number of words in Introduction: 769

Number of words in Discussion: 1643

JPET Fast Forward. Published on April 11, 2018 as DOI: 10.1124/jpet.118.247767
This article has not been copyedited and formatted. The final version may differ from this version.

List of non-standard abbreviations

ABT, 1-aminobenzotriazole; AUC, area under the plasma concentration-time curve; AUCR, ratio of the area under the plasma concentration-time curve; AUC_{po}, area under the plasma concentration-time curve of oral statin; AUC_{last}, area under the plasma concentration-time curve from time 0 to the last time point; $AUC_{0-\infty}$, area under the plasma concentration-time curve from time 0 to infinity; BCA, bicinchoninic acid; BCRP, breast cancer resistance protein; CL_{active}, active uptake clearance; CL_{diff}, passive diffusion clearance; $CL_{hepatic}$, hepatic clearance; CL_{iv}, intravenous clearance; C_{max}, maximum plasma concentration; CL_{renal}, renal clearance; DDI(s), drug-drug interaction(s); DPBS, Dulbecco's Phosphate Buffered Saline; ECCS, extended clearance classification system; F, oral bioavailability; F_a, fraction of drug absorbed; F_g, fraction of drug escaping intestinal extraction; F_h, fraction of drug escaping hepatic extraction; $f_{u,cell}$, fraction of unbound drug in the cell; $f_{u,med}$, nonspecific binding in the media; gmfe, geometric mean fold error; HEK293, human embryonic kidney 293 cells; IC_{50}, inhibitory constant (concentration at which 50% of total inhibitory effect is observed); IVIVE, *in vitro-in vivo* extrapolation; K_i, reversible inhibition constant; K_m, affinity constant; LC-MS/MS, liquid chromatography-tandem mass spectrometry; MRP2, multidrug resistance protein 2; NTCP, sodium taurocholate co-transporting polypeptide; OATP, organic anion transporting polypeptide; Q_h, hepatic blood flow; $t_{1/2}$, half-life; Vd_{ss}, volume of distribution; V_{max}, maximum uptake rate.

JPET Fast Forward. Published on April 11, 2018 as DOI: 10.1124/jpet.118.247767
This article has not been copyedited and formatted. The final version may differ from this version.

Abstract

Hepatic organic anion transporting polypeptides (OATP) 1B1 and 1B3 are clinically relevant transporters associated with significant drug-drug interactions (DDIs) and safety concerns. Given that OATP1Bs in cynomolgus monkey share >90% degree of gene and amino acid sequence identity with human orthologs, we evaluated the *in vitro–in vivo* translation of OATP1B-mediated DDI risk using this preclinical model. *In vitro* studies using cynomolgus monkey hepatocytes showed active uptake K_m values of 2.0 and 3.9 µM for OATP1B probe substrates, pitavastatin and rosuvastatin, respectively. Rifampicin inhibited pitavastatin and rosuvastatin active uptake in monkey hepatocytes with IC_{50} values of 3.0 and 0.54 µM, respectively, following pre-incubation with the inhibitor. Intravenous pharmacokinetics of $^2H_4$-pitavastatin and $^2H_6$-rosuvastatin (0.2 mg/kg) and the oral pharmacokinetics of cold probes (2 mg/kg) were studied in cynomolgus monkeys (n=4) without or with co-administration of single oral ascending doses of rifampicin (1, 3, 10 and 30 mg/kg). A rifampicin dose-dependent reduction in intravenous clearance of statins was observed. Additionally, oral pitavastatin and rosuvastatin plasma exposure increased up to 19- and 15-fold at the highest dose of rifampicin, respectively. Use of IC_{50} obtained following 1h pre-incubation with rifampicin (0.54 µM) predicted correctly the change in mean intravenous clearance and oral exposure of statins as a function of mean unbound C_{max} of rifampicin. This study demonstrates quantitative translation of *in vitro* OATP1B IC_{50} to predict DDIs using cynomolgus monkey as a preclinical model and provides further confidence in application of *in vitro* hepatocyte data for the prediction of clinical OATP1B-mediated DDIs.

JPET Fast Forward. Published on April 11, 2018 as DOI: 10.1124/jpet.118.247767
This article has not been copyedited and formatted. The final version may differ from this version.

Introduction

Drug-drug interactions (DDIs) involving hepatic organic anion transporting polypeptides (OATPs) are widely recognized as clinically important due to potential serious adverse events associated with them (Giacomini et al., 2010; Yoshida et al., 2012; El-Kattan et al., 2016; Galetin et al., 2017). Therefore, there is a strong need to quantitatively predict OATP-mediated DDIs early in candidate identification and drug development. Despite tremendous strides in establishing *in vitro* tools for assessing transporter role, confidence in quantitative prediction of transporter-mediated DDIs using *in vitro* data is arguably still low-to-moderate (Zamek-Gliszczynski et al., 2013; Jones et al., 2015; Yoshida et al., 2017).

Recently, cynomolgus monkey has been increasingly evaluated as a potential animal model for the assessment of OATP1B-mediated DDIs (Shen et al., 2013; Takahashi et al., 2013; Chu et al., 2015; Shen et al., 2015; Takahashi et al., 2016) due to >90% degree of gene and amino acid sequence identity between cynomolgus monkey and human orthologs for OATP1B uptake transporters (Ebeling et al., 2011; Shen et al., 2013; Takahashi et al., 2013). In addition to clinical drug probes, increasing evaluation of endogenous biomarkers for OATP1B DDIs (e.g., coproporhyrin I, bile acids) has been reported in this preclinical species (Chu et al., 2015; Watanabe et al., 2015; Shen et al., 2016; Thakare et al., 2017). DDIs reported in cynomolgus monkey for statins including rosuvastatin, pitavastatin and atorvastatin showed a good agreement in DDI classification (strong/moderate) relative to those observed in humans (Table S1, Supplementary Material). However, direct comparison of hepatic transporter-mediated DDIs between humans and monkeys may be challenging due to species differences in dosing regimen, transporter expression levels, activities and/or mechanisms involved in drug clearance. For instance, cynomolgus monkey liver expression of OATP1B1 and OAT1B3 was shown to be ~6- to 13-fold higher compared to human liver, respectively (Wang et al., 2015). In the case of OATP2B1 and sodium taurocholate co-transporting polypeptide (NTCP), the protein levels were either ~6-fold greater in human liver or comparable between the two species, respectively (Wang et al., 2015). Nevertheless, an *in vitro-in vivo* extrapolation (IVIVE) strategy using either static or physiologically-based pharmacokinetic (PBPK) modelling approaches accounting for the species differences could be employed for predicting clinical DDI risk.

JPET Fast Forward. Published on April 11, 2018 as DOI: 10.1124/jpet.118.247767
This article has not been copyedited and formatted. The final version may differ from this version.

Discrepancy in the translation of inhibitory potency (IC_{50} or K_i) to *in vivo* was reported for OATP inhibitors (Varma et al., 2012; Li et al., 2014; Yoshikado et al., 2017). For example, rifampicin *in vitro* K_i values were shown to be several fold higher than the *in vivo* K_i estimated from the clinical DDI data using mechanistic modelling (Varma et al., 2014; Barnett et al., 2017; Yoshikado et al., 2017). In addition, a number of studies demonstrated potentiation of OATP1B inhibition following pre-incubation with the inhibitor, trend particularly evident for cyclosporine (Amundsen et al., 2010; Gertz et al., 2013; Izumi et al., 2015; Takahashi et al., 2016; Pahwa et al., 2017) and incorporated in the recent FDA DDI guidance document (FDA, 2017). While the clinical DDIs with cyclosporine are well recovered with the IC_{50} obtained following pre-incubation (Gertz et al., 2013), there is limited understanding of the significance of pre-incubation in predicting DDIs of other inhibitor drugs. Additionally, recent studies reported substrate-dependence in the *in vitro* inhibition data for OATP1B inhibitors (Noé et al., 2007; Izumi et al., 2013). Due to the gaps in the available clinical DDI data, understanding of the translation of pre-incubation and substrate-dependent inhibition *in vitro* phenomena is still ambiguous.

Using cynomolgus monkey as a preclinical model, our goals in the current study are (i) to evaluate the predictability of OATP1B-mediated DDIs from *in vitro* inhibition data, and (ii) to understand the *in vivo* relevance of the effect of pre-incubation and substrate-dependency in rifampicin inhibition potential measured *in vitro*. In this study, the *in vitro* inhibition of transporter-mediated uptake of rosuvastatin and pitavastatin was investigated after incubation of cynomolgus monkey primary hepatocytes either with buffer or OATP inhibitors (rifampicin, cyclosporine and rifamycin SV). Prior to inhibition studies, an uptake kinetic characterization was performed for these two statins. Pitavastatin and rosuvastatin represent extended clearance classification system (ECCS) class 1B and class 3B, respectively, where OATP-mediated hepatic uptake is the rate-determining step in the systemic clearance in human (Varma et al., 2015; Varma et al., 2017). To allow separate evaluation of inhibitory effect of hepatic versus intestinal disposition, pharmacokinetics of both statins were studied following simultaneous intravenous (stable-labelled) and oral (cold) administration to cynomolgus monkey (n=4 animals) and over a wide rifampicin dose range (1-30 mg/kg). Finally, the extrapolation of rifampicin *in vitro* inhibition potency data obtained

JPET Fast Forward. Published on April 11, 2018 as DOI: 10.1124/jpet.118.247767
This article has not been copyedited and formatted. The final version may differ from this version.

using monkey hepatocytes to the *in vivo* changes in systemic clearance and plasma (i.v./oral) exposure of statins was evaluated.

JPET Fast Forward. Published on April 11, 2018 as DOI: 10.1124/jpet.118.247767
This article has not been copyedited and formatted. The final version may differ from this version.

Materials and Methods

Chemicals and Reagents. 3'-Phosphoadenosine-5'-phosphosulfate (PAPS), simvastatin, rifamycin SV, rifampicin, 1-aminobenzotriazole (ABT), cyclosporine A, naloxone, and tolbutamide were purchased from Sigma-Aldrich (St Louis, MO, USA). Deuterium labeled rifampicin ($^2H_8$-rifampicin) was obtained from ALSACHIM (Illkirch, Graffenstaden, France). Pitavastatin and rosuvastatin were purchased from Sequoia Research Products Ltd. (Oxford, UK). Deuterium labeled pitavastatin ($^2H_4$-pitavastatin) and rosuvastatin ($^2H_6$-rosuvastatin) were purchased from Clearsynth (Ontario, Canada). Atorvastatin was purchased from Toronto Research Chemicals (Toronto, Canada). InVitroGro CP hepatocyte medium and Torpedo antibiotic mix were purchased from InVitro GmbH (Frankfurt, Germany). Collagen I coated 24-well plates were obtained from VWR International (Leicestershire, UK). Cryopreserved cynomolgus monkey hepatocytes (female, pooled lot 10353012) were purchased from *In vitro* ADMET Laboratories, LLC (Columbia, Maryland). Bicinchoninic acid (BCA) protein assay kit was purchased from Life Technologies Ltd (Paisley, UK). Dulbecco's Phosphate Buffered Saline (DPBS) was obtained from Life Technologies Ltd (Paisley, UK). Acetonitrile, water, ammonium hydroxide were obtained from Fisher Scientific (Fair Lawn, New Jersey). Methanol was purchased from Fisher Scientific (Fair Lawn, New Jersey) and VWR International (Leicestershire, UK).

***In vitro* transport studies using monkey hepatocytes.** Cryopreserved cynomolgus monkey hepatocytes were thawed in pre-warmed InVitroGRO CP medium supplemented with torpedo antibiotic mix (2.2% v/v) according to the protocol from InVitro GmbH and cell viability was determined by Trypan Blue exclusion method. Hepatocyte suspension was diluted to 0.7 x 10^6 cells/mL with the prepared InVitroGRO CP medium and hepatocytes were seeded into collagen I-coated 24-well plates at a density of 350,000 cells per well. Cells were cultured for 4h at 37°C and 5% CO_2 in an incubator to allow attachment to the collagen. Cell confluency and monolayer formation was visually assessed before each experiment. Both the hepatic transporter uptake and its inhibition were investigated in plated cynomolgus monkey hepatocytes 4h post seeding using rosuvastatin and pitavastatin as probe substrates. Uptake was measured over a range of concentrations (0.1-0.3-1-3-10-30-100 µM) for 30, 60, 90 and 120 s at 37°C in triplicate to determine uptake kinetics, as described previously (Ménochet et al., 2012).

JPET Fast Forward. Published on April 11, 2018 as DOI: 10.1124/jpet.118.247767
This article has not been copyedited and formatted. The final version may differ from this version.

Inhibition of rosuvastatin and pitavastatin hepatic uptake by monkey hepatocytes was assessed in triplicate using the OATP inhibitor rifampicin (0.01-100 µM). In addition, inhibition with cyclosporine, (0.01-6 µM), and rifamycin SV (0.01-1000 µM) was investigated. Cyclosporine was included as a strong OATP inhibitor with evidence of pre-incubation effect in human *in vitro* systems (Gertz et al., 2013; Izumi et al., 2015), whereas rifamycin SV was considered as dual inhibitor of OATPs and NTCP (Bi et al., 2017). Rosuvastatin and pitavastatin concentrations used in the inhibition studies were 1 and 0.3 µM, respectively. The medium was removed after plating and cell monolayers were rinsed twice with pre-warmed DPBS. Effect of pre-incubation on the inhibition of hepatic uptake transporters in cynomolgus monkey hepatocytes was investigated by the addition of an inhibitor solution (400 µL) on the cell monolayer for 1h. In control group, pre-incubation was performed with DPBS containing 1 mM ABT. Following pre-incubation, cell monolayers were co-incubated with pre-warmed DPBS containing the inhibitor and the probe substrate for 3 min. This incubation was stopped by the removal of the medium and rinsing of the cell monolayers three times with 800 µL of ice cold DPBS. The cell monolayers were lysed in 200 µL ice cold deionised water for subsequent liquid chromatography-tandem mass spectrometry (LC-MS/MS) analysis. The *in vitro* sample preparation and LC-MS/MS analysis are described in Supplementary Material, Section S1. The LC-MS/MS conditions for each individual drug and their corresponding internal standards are detailed in Supplementary Material, Table S2.

***In vitro* data analysis.** Determination of the uptake kinetic parameters including the affinity constant K_m (µM), the maximum uptake rate V_{max} (pmol/min/10^6 cells), passive diffusion clearance CL_{diff} (µL/min/10^6 cells) and fraction unbound in the cell $f_{u,cell}$ for rosuvastatin and pitavastatin was performed using the two-compartment mechanistic model in Matlab 7.14 (2012) (The MathWorks,Inc., Natick, MA), as described previously (Ménochet et al., 2012). The active uptake clearance CL_{active} (µL/min/10^6 cells) was estimated from the V_{max} to K_m ratio. Parameter estimates were corrected for nonspecific binding in the media ($f_{u,med}$) which was calculated from the slope of the linear regression of the unbound substrate concentration extrapolated at t=0 vs the initial media concentration curve. The cellular concentrations were normalized for protein content as measured by the BCA protein assay kit at the end of incubation. Hepatocyte volume was set to 3.9 µL/10^6 cells as in rat (Reinoso et al., 2001); conversion of monkey hepatocyte data

JPET Fast Forward. Published on April 11, 2018 as DOI: 10.1124/jpet.118.247767
This article has not been copyedited and formatted. The final version may differ from this version.

expressed per mg protein to M cells was based on the 1:1 relationship between mg protein and M cells (in house data).

The data on substrate uptake (expressed as % control) at each inhibitor concentration were used to estimate the half-maximal inhibitory concentration IC_{50} (µM) of the inhibitors used. The analysis was performed in GraFit™ v6.0 (Erithacus Software Ltd, Horley, UK) by fitting a nonlinear least squares regression model as shown in Eq. 1 to the experimental data:

$$Substrate\ uptake\ (\%\ control) = \frac{Max - Min}{1 + \left(\frac{I}{IC_{50}}\right)^{s}} + Min \qquad (1)$$

where Max and Min represent the fitted maximum and minimum uninhibited uptake, respectively, I is the inhibitor concentration, corrected for $f_{u,med}$ (0.85, 0.7 and 0.95 for rifampicin, cyclosporine and rifamycin SV, respectively), and s is the slope factor. To increase the precision of the IC_{50} estimates, the minimum uptake was fixed to the experimental data. In all cases, the experimental data for minimum uptake was within 25% of the estimated value. Statistical analysis of the pre-incubation effect on IC_{50} was performed using a paired t-test where $p<0.05$ was considered as statistically significant.

In vivo **studies in cynomolgus monkeys.** All procedures performed on these animals were in accordance with regulations and established guidelines and were reviewed and approved by Pfizer Institutional Animal Care and Use Committee, and were conducted at Pfizer Groton (Connecticut, US). Male Cynomolgus macaque Mauritian monkeys (approximately 6 to 8.5 years of age) were used for these studies. A cross-over study design was employed, where the same four animals were dosed over a series of five studies, following a minimum one-week wash-out period between each study. One exception was the 3 mg/kg rifampicin dose group, where one of four monkeys was dosed only in that single study. Animals were provided a normal food schedule the day before the study (meals at 8:00 am and 11:00 am, with one treat daily) and were allowed free access to water. Animals were housed in metabolism cages during sample collection. On the day of the study, monkeys were fed at approximately 1h and 3h post-dose and allowed water *ad libitum*. Rifampicin was administered via oral gavage at 0 (blank vehicle), 1, 3, 10, and 30 mg/kg, at a dose volume of 2 ml/kg in a 0.5% (w/v) methylcellulose (in water) suspension. Rifampicin administration was immediately followed by oral doses of pitavastatin and rosuvastatin at a

dose of 2 mg/kg. Approximately one hour and 15 minutes following the oral rifampicin administration, $^{2}H_{4}$-pitavastatin and $^{2}H_{6}$-rosuvastatin were administered via intravenous (i.v.) bolus (cephalic vein), at dose of 0.2 mg/kg, in a dosing volume of 0.2 ml/kg; 2% dimethyl sulfoxide (DMSO) (v/v) and 98% of TRIS-buffered saline (pH ~7.7). All i.v. formulations were sterile filtered prior to administration. Serial blood samples were collected via the femoral vein into K_2EDTA tubes prior to dosing and then at 0.083, 0.25, 0.5, 0.75, 1, 2, 3, 5, 6, and 24 hours post i.v. dosing. Blood samples were stored on wet ice prior to being centrifuged to obtain plasma (3000 RPM, 10 minutes at 4°C; Jouan BR4i refrigerated centrifuge). Urine was also collected on wet ice, pre-dose and at intervals of 0 to 6 hours and 6 to 24 hours post-dose. Due to the potential instability of rifampicin and possible inter-conversion of lactone and acid forms of pitavastatin or rosuvastatin, each plasma and urine sample was equally divided into two aliquots prior to being stored frozen. The first aliquot was untreated matrix, while the second aliquot was added to an equal volume of 0.1 M sodium acetate buffer (pH 4). All urine and plasma samples, treated and untreated, were kept cold during collection, after which they were stored frozen at -20°C. The analysis of $^{2}H_{4}$-pitavastatin, $^{2}H_{6}$-rosuvastatin, pitavastatin, rosuvastatin and rifampicin in plasma samples by LC-MS/MS was described in Supplementary Material, Section 2. The analytes were monitored using multiple reaction monitoring with settings listed in Supplementary Material, Table S3.

Pharmacokinetic analysis and DDI predictions. Analyst 1.4.2 software (SCIEX, Framingham, MA) was used for LC-MS peak integration of plasma and urine samples. Raw data were imported into Watson LIMS™ version 7.4 (Thermo Fisher Scientific Inc, Waltham, MA) for standard curve regression and non-compartmental pharmacokinetic parameter calculations – area under the plasma concentration-time curve (AUC), maximum plasma concentration (C_{max}), intravenous clearance (CL_{iv}), volume of distribution (Vd_{ss}) and half-life ($t_{1/2}$). Other parameters were subsequently calculated on the basis of pharmacokinetic first principles. Oral bioavailability (F) of statins was described by Eq. 2:

$$F = F_a \cdot F_g \cdot F_h \quad (2)$$

where F_a, F_g and F_h represent fraction of drug absorbed, fraction of drug escaping intestinal and hepatic extraction, respectively. The F_h was described by Eq. 3.

JPET Fast Forward. Published on April 11, 2018 as DOI: 10.1124/jpet.118.247767
This article has not been copyedited and formatted. The final version may differ from this version.

$$F_h = 1 - \frac{CL_{hepatic}}{Q_h} \qquad (3)$$

where $CL_{hepatic}$ represents hepatic blood clearance (plasma $CL_{hepatic}$/blood-to-plasma ratio), and Q_h is hepatic blood flow in cynomolgus monkey (44 mL/min/kg) (Hosea et al., 2009). Measured blood-to-plasma ratios of rosuvastatin and pitavastatin in cynomolgus monkey were 0.55 and 0.58, respectively.

The ratio of the area under the plasma concentration-time curve (AUCR) of oral statins in the presence (AUC'_{po}) and absence (AUC_{po}) of rifampicin was predicted based on Eq 4.

$$AUCR = \frac{AUC'_{po}}{AUC_{po}} = \frac{F_a'}{F_a} \cdot \frac{F_g'}{F_g} \cdot \frac{F_h'}{F_h} \cdot \frac{(CL_{iv})}{(CL_{iv}')} \qquad (4)$$

where ′ indicates parameters in the presence of rifampicin. For the prediction purposes, it was assumed that rifampicin has no impact on F_a and F_g of both statins, and therefore F_a' and F_g' were the same as in the control phase. F_h' was estimated from the hepatic blood clearance in the presence of rifampicin ($CL_{hepatic}'$) as shown in Eq. 5.

$$F_h' = 1 - \frac{CL_{hepatic}'}{Q_h} \qquad (5)$$

The CL_{iv} of statins is the sum of hepatic and renal clearance and assuming uptake is the rate-determining step for hepatic clearance it can be expressed as shown in Eq. 6:

$$CL_{iv} = CL_{hepatic} + CL_{renal} = CL_{active} + CL_{diff} + CL_{renal} \qquad (6)$$

where CL_{renal}, CL_{active} and CL_{diff} represent renal, sinusoidal active uptake and passive diffusion clearance, respectively.

In vivo IC_{50} values were estimated using the Eq. 7 using unbound C_{max} of rifampicin ($[C_{u,max}]$) as independent variable and intravenous clearance of statins as the depending variable.

$$CL_{iv}' = \left[\frac{CL_{active}}{1 + \frac{[C_{u,max}]}{IC_{50}}} + CL_{diff}' \right] + CL_{renal}' \qquad (7)$$

CL_{diff} was obtained from the data in the presence of the highest rifampicin dose assuming complete inhibition of active hepatic uptake (Eq. 8). It was assumed that rifampicin had no impact on the passive

diffusion and renal clearance of both statins, and therefore CL_{diff}' and CL_{renal}' were the same as CL_{diff} and CL_{renal}.

$$CL_{diff} = CL_{iv(+30\,mg/kg\,rifampicin)} - CL_{renal} \quad (8)$$

Geometric mean fold error (gmfe) was calculated to assess the bias of the predicted rosuvastatin and pitavastatin AUCR across rifampicin dose range, as shown in Eq. 9 (Gertz et al., 2010).

$$gmfe = 10^{\frac{1}{N}\sum\left|\log\frac{predicted}{observed}\right|} \quad (9)$$

where N represents the number of observations.

JPET Fast Forward. Published on April 11, 2018 as DOI: 10.1124/jpet.118.247767
This article has not been copyedited and formatted. The final version may differ from this version.

Results

***In vitro* uptake kinetics of rosuvastatin and pitavastatin in monkey hepatocytes.** Uptake of rosuvastatin and pitavastatin (0.1 to 100 µM) was investigated after incubation with plated cynomolgus monkey hepatocytes and the kinetic parameters were estimated using the mechanistic two-compartment model. The measured $f_{u,med}$ was 0.83 and 0.99 for rosuvastatin and pitavastatin, respectively, which was used for correction of the initial media concentrations of both drugs. Kinetic profiles of both drugs in monkey hepatocytes demonstrated a saturable and nonsaturable uptake phase (Figure 1, Table 1). The K_m of rosuvastatin and pitavastatin were 3.29 and 1.99 µM, respectively. Although pitavastatin active uptake clearance was greater than for rosuvastatin (CL_{active} of 109 µL/min/10^6 cells *vs.* 98.3 µL/min/10^6 cells), the contribution of active process to total uptake was approximately 96% in case of rosuvastatin versus 80% for pitavastatin. The CL_{diff} was approximately 6-fold higher for pitavastatin (26.5 µL/min/10^6 cells) than in the case of rosuvastatin (4.27 µL/min/10^6 cells). Furthermore, the extent of intracellular binding differed between the two probes, as $f_{u,cell}$ was 0.25 and 0.024 for rosuvastatin and pitavastatin, respectively.

***In vitro* uptake inhibition potency of rifampicin and cyclosporine in monkey hepatocytes.** Both rifampicin and cyclosporine inhibited OATP-mediated rosuvastatin and pitavastatin uptake in a concentration-dependent manner (Figure 2). For rosuvastatin, up to 88% inhibition was observed after pre-incubation with rifampicin (Figure 2A). The uninhibited uptake of rosuvastatin (12%) was in close agreement with the contribution of passive diffusion (4%) estimated from the uptake kinetic study in monkey hepatocytes. The IC_{50} of rifampicin obtained after pre-incubation with buffer (1.14 µM) was reduced by approximately 2-fold after pre-incubation with rifampicin (0.54 µM) (Table 2). This marginal (2-fold) effect of pre-incubation on rifampicin potency seen with rosuvastatin reflects similar findings reported for this inhibitor in human OATP1B1 and OATP1B3 transfected HEK293 cells with estradiol-17β-glucuronide as a probe (2- and 3-fold increase in potency, details in Supplementary Table S4). Cyclosporine showed similar extent of maximal inhibition of rosuvastatin uptake in monkey hepatocytes at the highest concentration (Figure 2C). However, the increase in cyclosporine inhibition potency following pre-incubation was more pronounced (7-fold shift) (Table 2).

JPET Fast Forward. Published on April 11, 2018 as DOI: 10.1124/jpet.118.247767
This article has not been copyedited and formatted. The final version may differ from this version.

In the case of pitavastatin, maximal 55% inhibition of uptake was observed at the highest rifampicin concentration and after pre-incubation with inhibitor (Figure 2B). There was no significant change in the IC_{50} value after pre-incubation with rifampicin relative to pre-incubation with buffer (Table 2). This is in agreement with the data reported in HEK293 cells expressing cynomolgus monkey OATP1B1/1B3 using pitavastatin as a probe, where pre-incubation with inhibitor resulted in no significant change in rifampicin IC_{50} (Supplementary Table S4). Discrepancy between the uninhibited uptake (45%) and contribution of passive diffusion (20%) estimated from uptake kinetic data was apparent in case of pitavastatin. Cyclosporine also showed incomplete inhibition of pitavastatin uptake (Figure 2D), but in contrast to rifampicin its inhibitory potency increased 3.7-fold following pre-incubation with the inhibitor (Table 2). Additionally, reduction in the steepness of the IC_{50} curves was observed after pre-incubation in particular with cyclosporine (Figure 2C and D). DDI studies with rifamycin SV were also performed to elucidate the possible involvement of NTCP in pitavastatin uptake, which would not be inhibited by rifampicin. The maximum inhibition of pitavastatin uptake increased to 64% after pre-incubation with rifamycin SV, suggesting some contribution of NTCP in pitavastatin uptake in monkey hepatocytes (Figure S1, Supplementary Material). No effect of pre-incubation on rifamycin SV inhibition potency was observed in plated monkey hepatocytes (Table 2). Assuming almost complete inhibition of transporter-mediated uptake of pitavastatin at 1 mM rifamycin SV (Thakare et al., 2017), this uninhibited uptake should represent the contribution of passive diffusion to total cellular uptake, which in this case was higher compared with estimates obtained by mechanistic modelling of kinetic data done over short incubation times. Such incomplete inhibition of uptake for pitavastatin has previously been reported in monkey hepatocytes using rifampicin and cyclosporine (Takahashi et al., 2013) and in human hepatocytes using rifampicin (Pahwa et al., 2017) and may reflect the combination of passive diffusion and involvement of transporter uptake not inhibited by these inhibitors.

Dose-dependent effect of rifampicin on i.v. and oral pharmacokinetics of rosuvastatin and pitavastatin in monkeys. Intravenous pharmacokinetics of stable-labeled rosuvastatin and pitavastatin and the oral pharmacokinetics of cold rosuvastatin and pitavastatin were measured in cynomolgus monkeys after single oral ascending does of rifampicin (1 mg, 3 mg, 10 mg and 30 mg), and compared

with the vehicle only dosing (control). The plasma concentration-time profiles and the corresponding pharmacokinetic parameters are shown in Figure 3 and 4 and Table 3. Rosuvastatin i.v. clearance, when dosed along with 30 mg/kg rifampicin, decreased to almost 50% of control, while there was no significant change in the volume of distribution. This is in agreement with the previously reported marginal decrease in Vd_{ss} of i.v. rosuvastatin when given with a lower rifampicin dose in cynomolgus monkey (Chu et al., 2015). Oral AUC and C_{max} of rosuvastatin were increased up to 15-fold by the highest dose of rifampicin. In case of pitavastatin, reduction in i.v. clearance was more prominent (18.0 mL/min/kg versus 4.3 mL/min/kg), and the volume of distribution was reduced from 1.8 L/kg (control) to 0.55 L/kg (30 mg/kg rifampicin group). The decrease in intravenous clearance was accompanied by a significant decrease in Vd_{ss}, consistent with a previous report (Takahashi et al., 2013), and therefore, $t_{1/2}$ was not altered significantly by rifampicin. Rifampicin dose-dependent increase in oral pitavastatin plasma exposure was noted with AUC change of up to ~19-fold and C_{max} increase of up to ~12-fold at the highest dose tested (30 mg/kg) compared to the control group.

The lactone forms of orally administered pitavastatin and rosuvastatin were also measured in plasma samples. The plasma $AUC_{0-\infty}$ of the lactone forms in the absence and presence of rifampicin and the lactone-acid ratios are reported in the Supplementary Table S5 and S6, respectively. No significant increase in the overall lactone plasma $AUC_{0-\infty}$ was observed for rosuvastatin (Supplementary Table S5). In the case of pitavastatin lactone, a significant increase in its plasma $AUC_{0-\infty}$ was observed at 3 mg/kg rifampicin. No clear dose dependent trend in lactone $AUC_{0-\infty}$ of both statins was apparent. A significant increase in lactone-acid $AUC_{0-\infty}$ ratios was observed for rosuvastatin only at 1 mg/kg rifampicin relative to control, whereas no significant changes were seen for pitavastatin at any rifampicin dose (Supplementary Table S6). There was an apparent decrease in lactone-acid $AUC_{0-\infty}$ ratios for both statins particularly at the highest rifampicin doses. Previously a decrease and no change in lactone:acid ratio of pitavastatin (in human) and rosuvastatin (in cynomolgus monkey), respectively was observed in the presence of rifampicin (Prueksaritanont et al., 2014; Chu et al., 2015). Given that the AUC ratio of a metabolite to parent reflects both the formation and subsequent elimination of the metabolite (Houston, 1981), such behavior is not unexpected.

JPET Fast Forward. Published on April 11, 2018 as DOI: 10.1124/jpet.118.247767
This article has not been copyedited and formatted. The final version may differ from this version.

IVIVE of OATPs inhibition. *In vivo* inhibitory potency values estimated using unbound C_{max} of rifampicin were 0.99 ± 3.8 µM and 0.22 ± 0.14 µM against CL_{iv} of rosuvastatin and pitavastatin, respectively (Figure 6, Table 2). *In vitro* IC_{50} (0.54 µM), obtained in monkey hepatocytes following rifampicin pre-incubation and using rosuvastatin as probe substrate, described reasonably well rifampicin dose-dependent inhibition of rosuvastatin CL_{iv}. In contrast, *in vitro* IC_{50} obtained using pitavastatin as probe substrate did not recover the *in vivo* inhibition activity of rifampicin against pitavastatin CL_{iv}. However, *in vitro* IC_{50} generated using rosuvastatin described well the *in vivo* data of pitavastatin. Subsequently, *in vitro* IC_{50} value of 0.54 µM and inhibitor unbound C_{max} were employed to predict the rifampicin dose-dependent change in AUC of both statins dosed either intravenously or orally (Figure 7). The prediction bias calculated from the gmfe was <1.6-fold for both statins, with 78 and 88% of the predicted AUCR values within 2-fold of the observed data for rosuvastatin and pitavastatin, respectively. An apparent underprediction was noted for the rosuvastatin oral AUC ratio at higher doses of rifampicin. This is likely due to increased oral absorption as a result of inhibition of rosuvastatin intestinal efflux, which was not captured in the current prediction model (see Methods). To note, exploration of IVIVE using IC_{50} of 0.42 µM obtained in HEK293 cells expressing cOATP1B1 (lowest value compared to those obtained for other OATPs) and using rosuvastatin as an OATP probe (Shen et al., 2013) resulted in either no or marginal improvement in the prediction bias, highlighting the physiological relevance of monkey hepatocytes for comparison with the inhibition parameters obtained from the *in vivo* data in a top down manner.

The F_aF_g of rosuvastatin estimated from the intravenous and oral data of each study arm showed on average a 178% (2.8-fold) increase in rosuvastatin F_aF_g in monkeys receiving 30 mg/kg rifampicin relative to the control arm; this trend was not evident for pitavastatin. Correction of the average predicted AUCR values shown in Figure 7A by this increase in F_aF_g reduced the underprediction of the magnitude of rosuvastatin DDI at the highest dose of rifampicin (data not shown).

Discussion

In comparison to the increased success of quantitative prediction of CYP-mediated DDIs, the confidence in the successful prediction of OATP-mediated DDIs using *in vitro* data is still low (Gertz et al., 2013; Prueksaritanont et al., 2014; Jones et al., 2015; Bi et al., 2017; Yoshida et al., 2017). Therefore, the objective of our study was to evaluate the IVIVE of OATP inhibition potential using cynomolgus monkey as a preclinical model and to gain confidence in mechanistic translational approach to predict clinical DDIs mediated by these transporters. Furthermore, it was aimed at improving our understanding of the utility of the cynomolgus monkey as a model for human to drive evaluation of clearance mechanisms (rate-determining step) and DDI risk. Collective results suggest that quantitative OATP1B DDI predictions can be made from *in vitro* IC_{50} measured in primary hepatocytes using multiple probe substrates following pre-incubation with the inhibitor.

In the current study, both rosuvastatin and pitavastatin showed a high affinity for uptake transport in monkey hepatocytes (Table 1). Rosuvastatin CL_{active} was approximately 4-fold greater in the current monkey donor investigated compared to the previous data (Shen et al., 2013), possibly reflecting donor differences in the transporter activity, as the estimated K_m values were comparable. Although CL_{diff} was about 6-fold greater in the donor used in the current study, contribution of the passive process to the overall uptake of rosuvastatin (4.2%) was in agreement with previous reports in monkey hepatocytes (Shen et al., 2013).

In this study, the effect of pre-incubation on the inhibition of OATP-mediated rosuvastatin and pitavastatin uptake in monkey hepatocytes was investigated using prototypical inhibitors rifampicin and cyclosporine. In contrast to the marginal decrease in rifampicin IC_{50} after pre-incubation, more pronounced increase in cyclosporine potency (up to 7-fold) was seen regardless of the substrate probe used. This clear pre-incubation effect on cyclosporine inhibition potency demonstrated here in monkey hepatocytes is in agreement with previous literature reports on this inhibitor. But the reported magnitude of shift in cyclosporine potency varied between *in vitro* systems and probes used (Table S4, Supplementary Material), with up to 22- and 23-fold increase in cyclosporine potency noted after pre-incubation in human

and monkey OATP1B1 transfected HEK293 cells, respectively, highlighting that the effect of pre-incubation on the potency of OATP inhibitors is dependent not only on the substrate used but also on the cellular system investigated.

Incomplete inhibition of uptake was observed for pitavastatin in the current study. As a number of reports demonstrated the contribution of sodium-dependent NTCP to the uptake of pitavastatin and rosuvastatin in human (Bi et al., 2013; Bi et al., 2017) and monkey hepatocytes (Thakare et al., 2017), pitavastatin uptake was further evaluated in the presence of rifamycin SV. Although rifamycin SV increased the maximal inhibition of pitavastatin uptake in monkey hepatocytes, incomplete inhibition of uptake was still evident, highlighting potentially lower transporter activity and/or higher passive contribution in the pooled donor investigated.

The quantitative translation of interaction noted in monkeys to humans may not be straightforward due to possible species difference in the multiple mechanisms involved in the clearance. However, several recent reports suggested good agreement between cynomolgus monkey and human in the magnitude of DDIs with rifampicin as an OATP inhibitor (Shen et al., 2013; Watanabe et al., 2015). In this study, rifampicin showed a dose-dependent effect with no further change in statins pharmacokinetics between rifampicin doses of 10 and 30 mg/kg in monkeys. The unbound C_{max} of rifampicin achieved (~2 to 7 μM) at these doses are comparable to the unbound C_{max} in human following single 600 mg dose (Varma et al., 2012; Prueksaritanont et al., 2014; Yoshikado et al., 2017). However, the magnitude of change in the oral AUC for both statins observed in the cynomolgus monkeys (~15 to 20-fold, Table 3) is much higher than noted in humans (AUC ratio ~5) (Prueksaritanont et al., 2014). In contrast, an earlier study showed ~3-fold increase in oral rosuvastatin AUC in cynomolgus monkey with rifampicin dose of 15 mg/kg orally (Shen et al., 2013). While the reasons for such a difference are not apparent, a relatively smaller magnitude of rosuvastatin DDI in human may be attributed to the contribution of hepatic OATP2B1 which is not affected by rifampicin at *in vivo* relevant plasma concentrations (OATP2B1 *in vitro* IC_{50}>60 μM). However, the contribution of OATP2B1 to rosuvastatin hepatic uptake in monkey is likely to be minor because of its relatively low expression in cynomolgus liver (Wang et al., 2015). In addition to OATPs,

both rosuvastatin and pitavastatin are substrates of efflux transporters such as multidrug resistance protein 2 (MRP2) and breast cancer resistance protein (BCRP) (Prueksaritanont et al., 2014; Lee et al., 2015). As rifampicin is also a substrate of OATP1Bs (Yamaguchi et al., 2011), its inhibitory effect on the biliary efflux of rosuvastatin and pitavastatin was considered. Previously, Chu et al. (2015) showed relatively weak inhibition of cMRP2 by rifampicin in HEK293 cells (IC_{50} of 118 µM). Assuming the reported unbound liver-to-plasma concentration ratio (Kp_{uu}) of 3.3 for rifampicin in humans (Chu et al., 2015) is comparable to that in cynomolgus monkey, the IC_{50} for cMRP2 is much higher than the estimated rifampicin unbound liver concentrations (approximately 23 µM at the highest rifampicin dose used), suggesting that the increase in plasma exposure of both statins is unlikely to be caused by MRP2 inhibition. In case of potential MRP2 inhibition, expectation is that liver AUC will change, consistent with an understanding of the rate-determining processes that affect hepatic exposure of these drugs (Tsamandouras et al., 2015).

The increase in F_aF_g of rosuvastatin seen in this study is most likely attributed to the effect of rifampicin on intestinal BCRP. Rosuvastatin absorption in humans is approximately 50% of the oral dose (Martin et al., 2003), whereas only ~20% was noted in monkeys (control arm). This difference in F_aF_g values suggests species differences in the expression of the intestinal transporters including BCRP. This is supported by previous reports of generally greater mRNA expression of intestinal efflux transporters in cynomolgus monkey relative to human (60-fold difference in the case of BCRP) (Takahashi et al., 2008). While, we cannot assess the differential effects of OATP2B1 uptake versus BCRP efflux definitively, increased absorption following rifampicin administration implies that BCRP efflux plays a prominent role in the oral absorption of rosuvastatin in monkey. In contrast, pitavastatin is a highly permeable drug and the F_aF_g (~0.7 in control arm) is not expected to be limited by intestinal efflux (El-Kattan et al., 2016). Taken together, the current monkey study suggests potential contribution of intestinal efflux inhibition to the rifampicin-rosuvastatin DDIs.

The rich dataset of rifampicin dose-dependent effect on two statins simultaneously dosed i.v. and orally was leveraged to investigate the IVIVE of OATP1B-mediated DDIs. The *in vivo* IC_{50} values, estimated

JPET Fast Forward. Published on April 11, 2018 as DOI: 10.1124/jpet.118.247767
This article has not been copyedited and formatted. The final version may differ from this version.

using intravenous clearance of rosuvastatin/pitavastatin and unbound C_{max} of rifampicin, were within 2.5-fold of the *in vitro* IC_{50} (0.54 µM) obtained following pre-incubation with rifampicin and using rosuvastatin as probe substrate in primary monkey hepatocytes. This *in vitro* IC_{50} predicted the AUCR of both statins after i.v. and oral dosing with high accuracy (minimum 78% within 2-fold of the observed data), when employing the static mechanistic model (Eq. 7). In contrast, the *in vitro* IC_{50} obtained under all other experimental conditions (Table 2) considerably underpredicted the fold change in the AUC of statins investigated. Consistent with the IVIVE noted here in monkey, Varma et al. demonstrated that similar inhibition potency (0.5 µM), obtained using OATP1B1-transfected cells, correctly predicted rifampicin clinical DDIs when using a static mechanistic model (>85% within 2-fold of observed AUC ratios, n=22) (Varma et al., 2014). Overall, the current monkey study validates mechanistic translational framework to predict OATP1B-mediated DDIs in human.

Substrate-dependent inhibition was argued as a potential cause for concern in prospective prediction of OATP1B-mediated interactions (Noé et al., 2007; Izumi et al., 2013; Zamek-Gliszczynski et al., 2013). We report almost 6-fold difference in rifampicin IC_{50} measured with pre-incubation when using rosuvastatin (0.54 µM) *vs.* pitavastatin (3.0 µM) (Table 2). Interestingly, the change in i.v. clearance and oral exposure of both rosuvastatin and pitavastatin are recovered well only by the rifampicin *in vitro* IC_{50} measured against rosuvastatin (Figure 6 and 7). Based on these findings, it can be inferred that, (i) substrate-dependent inhibitory potency noted *in vitro* may not translate to differences *in vivo*, (ii) IC_{50} measured following pre-incubation with inhibitor is needed for quantitative prediction of OATP-mediated DDIs, and (iii) *in vitro* inhibition studies should consider more than one probe substrates and the most potent measurement should be employed for reliable prospective predictions. Of note, plasma coproporphyrins (I and III) have recently been described as selective OATP1B biomarkers in both cynomolgus monkey and human (Shen et al., 2016; Barnett et al., 2017). Therefore, the coordinated use of the cynomolgus monkey (pre-human dosing), with measurements of changes in biomarker exposure in Phase 1, could be leveraged to quickly discharge OATP1B DDI risk. Given that current regulatory agency-driven OATP1B DDI risk analyses are conservative, and present a relatively high false positive rate (~30%) (Vaidyanathan et al., 2016), consideration of such approaches is warranted.

JPET Fast Forward. Published on April 11, 2018 as DOI: 10.1124/jpet.118.247767
This article has not been copyedited and formatted. The final version may differ from this version.

In summary, our studies using the cynomolgus monkey as a model demonstrated a rational translation of *in vitro* inhibition potency in predicting OATP1B DDIs. Rifampicin *in vitro* inhibition potency measured using monkey hepatocytes was influenced by a pre-incubation step and/or the probe substrate employed. However, *in vivo* IC_{50} values obtained from the change in rosuvastatin or pitavastatin i.v. clearance as a function of rifampicin unbound C_{max} were not statistically different. Additionally, the most potent IC_{50} obtained under pre-incubation conditions provided good quantitative predictions of fold-changes in plasma AUC for both statins following oral administration. Collectively, these findings suggest the need for employing multiple probe substrates and a pre-incubation step when conducting *in vitro* inhibition studies. Finally, this study emphasizes further the utility of cynomolgus monkey as a preclinical model in supporting the early assessment of OATP-mediated DDI risk.

Acknowledgements

Authors would like to thank Drs. R. Scott Obach, Emi Kimoto, Elaine Tseng and Theunis Goosen (Pfizer Inc.) for valuable inputs during this work. Sangwoo Ryu and Keith Riccardi (Pfizer Inc.) are acknowledged for conducting plasma protein binding measurements.

Authorship Contribution

Participated in research design: Ufuk, Kosa, Gao, Bi, Rodrigues, Tremaine, Varma, Houston, and Galetin

Conducted experiments: Ufuk, Kosa, Gao, Bi, Modi, Gates

Contributed new reagents or analytical tools: Gao

Performed data analysis: Ufuk, Kosa, Varma, Houston, and Galetin

Wrote or contributed to the writing of the manuscript: Ufuk, Kosa, Gao, Modi, Gates, Rodrigues, Tremaine, Varma, Houston, and Galetin

References

Amundsen R, Christensen H, Zabihyan B and Asberg A (2010) Cyclosporine A, but not tacrolimus, shows relevant inhibition of organic anion-transporting protein 1B1-mediated transport of atorvastatin. *Drug Metab Dispos* **38:**1499-1504.

Barnett S, Ogungbenro K, Menochet K, Shen H, Lai Y, Humphreys WG and Galetin A (2017) Gaining mechanistic insight into coproporphyrin I as endogenous biomarker for OATP1B-mediated drug-drug interactions using population pharmacokinetic modelling and simulation. *Clin Pharmacol Ther*.doi:10.1002/cpt.983

Bi YA, Qiu X, Rotter CJ, Kimoto E, Piotrowski M, Varma MV, Ei-Kattan AF and Lai Y (2013) Quantitative assessment of the contribution of sodium-dependent taurocholate co-transporting polypeptide (NTCP) to the hepatic uptake of rosuvastat in, pitavastatin and fluvastatin. *Biopharm Drug Dispos* **34:**452-461.

Bi YA, Scialis RJ, Lazzaro S, Mathialagan S, Kimoto E, Keefer J, Zhang H, Vildhede AM, Costales C, Rodrigues AD, Tremaine LM and Varma MVS (2017) Reliable Rate Measurements for Active and Passive Hepatic Uptake Using Plated Human Hepatocytes. *Aaps j* **19:**787-796.

Chu X, Shih SJ, Shaw R, Hentze H, Chan GH, Owens K, Wang S, Cai X, Newton D, Castro-Perez J, Salituro G, Palamanda J, Fernandis A, Ng CK, Liaw A, Savage MJ and Evers R (2015) Evaluation of cynomolgus monkeys for the identification of endogenous biomarkers for hepatic transporter inhibition and as a translatable model to predict pharmacokinetic interactions with statins in humans. *Drug Metab Dispos* **43:**851-863.

Ebeling M, Kung E, See A, Broger C, Steiner G, Berrera M, Heckel T, Iniguez L, Albert T, Schmucki R, Biller H, Singer T and Certa U (2011) Genome -based analysis of the nonhuman primate Macaca fascicularis as a model for drug safety assessment. *Genome Res* **21:**1746-1756.

El-Kattan AF, Varma MV, Steyn SJ, Scott DO, Maurer TS and Bergman A (2016) Projecting ADME Behavior and Drug-Drug Interactions in Early Discovery and Development: Application of the Extended Clearance Classification System. *Pharm Res* **33:**3021-3030.

FDA (2017) In vitro m etabolism- and transporter-mediated drug-drug interaction studies guidance for industry. <https://www.fda.gov/downloads/Drugs/Guidances/UCM581965.pdf>.

Galetin A, Zhao P and Huang SM (2017) Physiologically Based Pharmacokinetic Modeling of Drug Transporters to Facilitate Individualized Dose Prediction. *J Pharm Sci* **106:**2204-2208.

Gertz M, Cartwright CM, Hobbs MJ, Kenworthy KE, Rowland M, Houston JB and Galetin A (2013) Cyclosporine inhibition of hepatic and intestinal CYP3A4, uptake and efflux transporters: application of PBPK modeling in the assessment of drug-drug interaction potential. *Pharm Res* **30:**761-780.

Gertz M, Harrison A, Houston JB and Galetin A (2010) Prediction of human intestinal first -pass metabolism of 25 CYP3A substrates from in vitro clearance and permeability data. *Drug Metab Dispos* **38:**1147-1158.

Giacomini KM, Huang SM, Tweedie DJ, Benet LZ, Brouwer KL, Chu X, Dahlin A, Evers R, Fischer V, Hillgren KM, Hoffmaster KA, Ishikawa T, Keppler D, Kim RB, Lee CA, Niemi M, Polli JW, Sugiyama Y, Swaan PW, Ware JA, Wright SH, Yee SW, Zamek-Gliszczynski MJ and Zhang L (2010) Membrane transporters in drug de velopment. *Nat Rev Drug Discov* **9:**215-236.

Hosea NA, Collard WT, Cole S, Maurer TS, Fang RX, Jones H, Kakar SM, Nakai Y, Smith BJ, Webster R and Beaumont K (2009) Prediction of human pharmacokinetics from preclinical information: comparative accuracy of quantitative prediction approaches. *J Clin Pharmacol* **49:**513-533.

Houston JB (1981) Drug metabolite kinetics. *Pharmacol Ther* **15:**521-552.

Izumi S, Nozaki Y, Komori T, Maeda K, Takenaka O, Kusano K, Yoshimura T, Kusuhara H and Sugiyama Y (2013) Substrate -dependent inhibition of organic anion transporting polypeptide 1B1: comparative analysis with prototypical probe substrates estradiol-17beta-glucuronide, estrone-3-sulfate, and sulfobromophthalein. *Drug Metab Dispos* **41:**1859-1866.

Izumi S, Nozaki Y, Maeda K, Komori T, Takenaka O, Kusuhara H and Sugiyama Y (2015) Investigation of the impact of substrate selection on in vitro organic anion transporting polypeptide 1B1 inhibition profiles for the prediction of drug-drug interactions. *Drug Metab Dispos* **43:**235-247.

Jones HM, Chen Y, Gibson C, Heimbach T, Parrott N, Peters SA, Snoeys J, Upreti VV, Zheng M and Hall SD (2015) Physiologically based pharmacokinetic modeling in drug discovery and development: a pharmaceutical industry perspective. *Clin Pharmacol Ther* **97:**247-262.

Lee CA, O'Connor MA, Ritchie TK, Galetin A, Cook JA, Ragueneau-Majlessi I, Ellens H, Feng B, Taub ME, Paine MF, Polli JW, Ware JA and Zamek-Gliszczynski MJ (2015) Breast cancer resistance protein (ABCG2) in clinical pharmacokinetics and drug interaction s: practical recommendations for clinical victim and perpetrator drug-drug interaction study design. *Drug Metab Dispos* **43:**490-509.

Li R, Barton HA and Varma MV (2014) Prediction of pharmacokinetics and drug -drug interactions when hepatic transporters are involved. *Clin Pharmacokinet* **53:**659-678.

Martin PD, Warwick MJ, Dane AL, Brindley C and Short T (2003) Absolute oral bioavailability of rosuvastatin in healthy white adult male volunteers. *Clin Ther* **25:**2553-2563.

Ménochet K, Kenworthy KE, Houston JB and Galetin A (2012) Simultaneous assessment of uptake and metabolism in rat hepatocytes: a comprehensive mechanistic model. *J Pharmacol Exp Ther* **341:**2-15.

Noé J, Portmann R, Brun ME and Funk C ﹙2007﹚ Substrate-dependent drug-drug interactions between gemfibrozil, fluvastatin and other organic anion-transporting peptide (OATP) substrates on OATP1B1, OATP2B1, and OATP1B3. *Drug Metab Dispos* **35:**1308-1314.

Pahwa S, Alam K, Crowe A, Farasyn T, Neuhoff S, Hatley O, Ding K and Yue W (2017) Pretreatment With Rifampicin and Tyrosine Kinase Inhibitor Dasatinib Potentiates the Inhibitory Effects Toward OATP1B1- and OATP1B3-Mediated Transport. *J Pharm Sci* **106:**2123-2135.

Prueksaritanont T, Chu X, Evers R, Klopfer SO, Caro L, Kothare PA, Dempsey C, Rasmussen S, Houle R, Chan G, Cai X, Valesky R, Fraser IP and Stoch SA (2014) Pitavastatin is a more sensitive and selective organic anion-transporting polypeptide 1B clinical probe than rosuvastatin. *Br J Clin Pharmacol* **78:**587-598.

Reinoso RF, Telfer BA, Brennan BS and Rowland M (2001) Uptake of teicoplanin by isolated rat hepatocytes: comparison with in vivo hepatic distribution. *Drug Metab Dispos* **29:**453-459.

Shen H, Dai J, Liu T, Cheng Y, Chen W, Freeden C, Zhang Y, Humphreys WG, Marathe P and Lai Y (2016) Coproporphyrins I and III as Functional Markers of OATP1B Activity: In Vitro and In Vivo Evaluation in Preclinical Species. *J Pharmacol Exp Ther* **357:**382-393.

Shen H, Su H, Liu T, Yao M, Mintier G, Li L, Fancher RM, Iyer R, Marathe P, Lai Y and Rodrigues AD (2015) Evaluation of rosuvastatin as an organic anion transporting polypeptide (OATP) probe substrate: in vitro transport and in vivo disposition in cynomolgus monkeys. *J Pharmacol Exp Ther* **353:**380-391.

Shen H, Yang Z, Mintier G, Han YH, Chen C, Balimane P, Jemal M, Zhao W, Zhang R, Kallipatti S, Selvam S, Sukrutharaj S, Krishnamurthy P, Marathe P and Rodrigues AD (2013) Cynomolgus monkey as a potential model to assess drug interactions involving hepatic organic anion transporting polypeptides: in vitro, in vivo, and in vitro-to-in vivo extrapolation. *J Pharmacol Exp Ther* **344:**673-685.

Takahashi M, Washio T, Suzuki N, Igeta K, Fujii Y, Hayashi M, Shirasaka Y and Yamashita S (2008) Characterization of gastrointestinal drug absorption in cynomolgus monkeys. *Mol Pharm* **5:**340-348.

Takahashi T, Ohtsuka T, Uno Y, Utoh M, Yamazaki H and Kume T (2016) Pre -incubation with cyclosporine A potentiates its inhibitory effects on pitavastatin uptake mediated by recombinantly expressed cynomolgus monkey hepatic organic anion transporting polypeptide. *Biopharm Drug Dispos* **37:**479-490.

Takahashi T, Ohtsuka T, Yoshikawa T, Tatekawa I, Uno Y, Utoh M, Yamazaki H and Kume T (2013) Pitavastatin as an in vivo probe for studying hepatic organic anion transporting polypeptide-mediated drug-drug interactions in cynomolgus monkeys. *Drug Metab Dispos* **41:**1875-1882.

Thakare R, Gao H, Kosa RE, Bi YA, Varma MVS, Cerny MA, Sharma R, Kuhn M, Huang B, Liu Y, Yu A, Walker GS, Niosi M, Tremaine L, Alnouti Y and Rodrigues AD (2017) Leveraging of Rifampicin-Dosed Cynomolgus Monkeys to Identify Bile Acid 3-O-Sulfate Conjugates as Potential Novel Biomarkers for Organic Anion-Transporting Polypeptides. *Drug Metab Dispos* **45:**721-733.

Tsamandouras N, Dickinson G, Guo Y, Hall S, Rostami-Hodjegan A, Galetin A and Aarons L (2015) Development and Application of a Mechanistic Pharmacokinetic Model for Simvastatin and its Active Metabolite Simvastatin Acid Using an Integrated Population PBPK Approach. *Pharm Res* **32:**1864-1883.

Vaidyanathan J, Yoshida K, Arya V and Zhang L (2016) Comparing Various In Vitro Prediction Criteria to Assess the Potential of a New Molecular Entity to Inhibit Organic Anion Transporting Polypeptide 1B1. *J Clin Pharmacol* **56 Suppl 7:**S59-72.

Varma MV, Bi YA, Kimoto E and Lin J (2014) Quantitative prediction of transporter - and enzyme-mediated clinical drug-drug interactions of organic anion-transporting polypeptide 1B1 substrates using a mechanistic net-effect model. *J Pharmacol Exp Ther* **351:**214-223.

Varma MV, El ¡Kattan AF, Feng B, Steyn SJ, Maurer TS, Scott DO, Rodrigues AD and Tremaine LM (2017) Extended Clearance Classification System (ECCS) informed approach for evaluating investigational drugs as substrates of drug transporters. *Clin Pharmacol Ther* **102:**33-36.

Varma MV, Lai Y, Feng B, Litchfield J, Goosen TC and Bergman A (2012) Physiologically based modeling of pravastatin transporter-mediated hepatobiliary disposition and drug-drug interactions. *Pharm Res* **29:**2860-2873.

Varma MV, Steyn SJ, Allerton C and El-Kattan AF (2015) Predicting Clearance Mechanism in Drug Discovery: Extended Clearance Classification System (ECCS). *Pharm Res* **32:**3785-3802.

Wang L, Prasad B, Salphati L, Chu X, Gupta A, Hop CE, Evers R and Unadkat JD (2015) Interspecies variability in expression of hepatobiliary transporters across human, dog, monkey, and rat as determined by quantitative proteomics. *Drug Metab Dispos* **43:**367-374.

Watanabe M, Watanabe T, Yabuki M and Tamai I (2015) Dehydroepiandrosterone sulfate, a useful endogenous probe for evaluation of drug-drug interaction on hepatic organic anion transporting polypeptide (OATP) in cynomolgus monkeys. *Drug Metab Pharmacokinet* **30:**198-204.

Yamaguchi H, Takeuchi T, Okada M, Kobayashi M, Unno M, Abe T, Goto J, Hishinuma T, Shimada M and Mano N (2011) Screening of antibiotics that interact with organic anion -transporting polypeptides 1B1 and 1B3 using fluorescent probes. *Biol Pharm Bull* **34:**389-395.

Yoshida K, Maeda K and Sugiyama Y (2012) Transporter -mediated drug--drug interactions involving OATP substrates: predictions based on in vitro inhibition studies. *Clin Pharmacol Ther* **91:**1053-1064.

Yoshida K, Zhao P, Zhang L, Abernethy DR, Rekic D, Reynolds KS, Galetin A and Huang SM (2017) In Vitro-In Vivo Extrapolation of Metabolism- and Transporter-Mediated Drug-Drug Interactions-Overview of Basic Prediction Methods. *J Pharm Sci* **106:**2209-2213.

Yoshikado T, Maeda K, Furihata S, Terashima H, Nakayama T, Ishigame K, Tsunemoto K, Kusuhara H, Furihata KI and Sugiyama Y (2017) A Clinical Cassette Dosin g Study for Evaluating the Contribution of Hepatic OATPs and CYP3A to Drug-Drug Interactions. *Pharm Res* **34:**1570-1583.

Zamek-Gliszczynski MJ, Lee CA, Poirier A, Bentz J, Chu X, Ellens H, Ishikawa T, Jamei M, Kalvass JC, Nagar S, Pang KS, Korzekwa K, Swaan PW, Taub ME, Zhao P and Galetin A (2013) ITC recommendations for transporter kinetic parameter estimation and translational modeling of transport-mediated PK and DDIs in humans. *Clin Pharmacol Ther* **94:**64-79.

Footnote

AU was supported by a consortium of pharmaceutical companies (Eli Lilly, Pfizer, GlaxoSmithKline) within the Centre for Applied Pharmacokinetic Research at the University of Manchester.

Figure Legends

Figure 1. Uptake kinetic profiles of rosuvastatin (A) and pitavastatin (B) measured in cryopreserved cynomolgus monkey hepatocytes plated for 4h. Symbols represent the observed total uptake. Solid, dashed and dotted lines represent the predicted total, active and passive diffusion related uptake, respectively.

Figure 2. Rifampicin (A-B) and cyclosporine (C-D) concentration-dependent inhibition of rosuvastatin (A-C) and pitavastatin (B-D) as OATP substrates in cryopreserved cynomolgus monkey hepatocytes plated for 4h. Pre-incubation with either buffer or inhibitor (rifampicin 0.01-100 µM, cyclosporine 0.01-6 µM) was performed for 1h prior to co-incubation with the inhibitor and the probe substrates. Data represent mean ± SD of at least triplicate measurements.

Figure 3. Effect of single ascending oral doses of rifampicin on the intravenous and oral pharmacokinetics of rosuvastatin in cynomolgus monkey. Plasma concentration-time profiles of i.v. $^{2}H_{6}$-rosuvastatin (A) and oral cold rosuvastatin (B), and the estimated pharmacokinetics (C) are depicted. Pharmacokientics parameters were estimated with each monkey serving as its own control. Data represent mean and s.d. (n=4). One-way ANOVA with Dunnett's multiple comparisons test was employed to test significance with *p<0.05 and **p<0.01.

Figure 4. Effect of single ascending oral doses of rifampicin on the intravenous and oral pharmacokinetics of pitavastatin in cynomolgus monkey. Plasma concentration-time profiles of i.v. $^{2}H_{4}$-pitavastatin (A) and oral cold rosuvastatin (B), and the estimated pharmacokinetics (C) are depicted. Pharmacokientics parameters were estimated with each monkey serving as its own control. Data represent mean and s.d. (n=4). One-way ANOVA with Dunnett's multiple comparisons test was employed to test significance with *p<0.05 and **p<0.01.

Figure 5. Rifampicin mean unbound plasma concentration-time profiles at different doses following oral administration in cynomolgus monkey. Horizontal lines represent *in vitro* IC_{50} values estimated using

rosuvastatin and pitavastatin as probe substrates following pre-incubation with buffer or rifampicin (Table 2).

Figure 6. IVIVE of hepatic uptake inhibition by rifampicin in cynomolgus monkey. Plots depict rifampicin plasma concentration-dependent inhibition of intravenous clearance of rosuvastatin (A) and pitavastatin (B). Data were fitted to Eq. 7 to estimate *in vivo* IC_{50} with each statin (red curves with shaded area – 95% CI). Additionally, change in intravenous clearance was predicted using *in vitro* IC_{50} obtained in monkey hepatocytes following pre-incubation with rifampicin with rosuvastatin as a probe (green curve). Vertical lines represent *in vivo* and *in vitro* IC_{50} values (Table 2).

Figure 7. Predicted versus observed interactions between rifampicin and rosuvastatin (A) or pitavastatin (B), when administered with single ascending oral doses of rifampicin. Change in exposure (AUC ratio) of intravenous (open points) and oral (closed points) statins was predicted based on eqs. 4-7 using the measured unbound C_{max} of rifampicin and *in vitro* IC_{50} of 0.54 µM. Each monkey served as its own control in calculating the AUCR. Solid and dotted lines represent the line of unity and 2-fold error, respectively.

JPET Fast Forward. Published on April 11, 2018 as DOI: 10.1124/jpet.118.247767
This article has not been copyedited and formatted. The final version may differ from this version.

Table 1

Uptake kinetic parameters of rosuvastatin and pitavastatin estimated in plated cynomolgus monkey hepatocytes using a mechanistic two-compartment model

Drug	K_m	V_{max}	$f_{u,cell}$	CL_{diff}	CL_{active}
	µM	pmol/min/10^6 cells		µL/min/10^6 cells	
Rosuvastatin	3.29 ± 0.45	323 ± 44	0.25 ± 0.08	4.27 ± 1.07	98.3
Pitavastatin	1.99 ± 0.31	217 ± 34	0.025 ± 0.009	26.50 ± 2.74	109

JPET Fast Forward. Published on April 11, 2018 as DOI: 10.1124/jpet.118.247767
This article has not been copyedited and formatted. The final version may differ from this version.

Table 2

In vitro IC_{50} of rifampicin on the OATP-mediated uptake of rosuvastatin and pitavastatin with or without pre-incubation in cryopreserved plated cynomolgus monkey hepatocytes; and the in vivo IC_{50} estimated based on change in intravenous clearance for these two statins

Substrate	**Inhibitor**	***In vitro* IC_{50} (μM)**		***In vivo* IC_{50} (μM)**
		Pre-incubation with buffer	Pre-incubation with inhibitor	
Rosuvastatin	Rifampicin	1.14 ± 0.34**	0.54 ± 0.13**	0.99 ± 3.80
	Cyclosporine	0.72 ± 0.04**	0.10 ± 0.04 **	-
Pitavastatin	Rifampicin	3.80 ± 1.82	2.98 ± 0.78	0.22 ± 0.14
	Cyclosporine	0.78 ± 0.14**	0.21 ± 0.06**	-
	Rifamycin SV	6.17 ± 0.96	4.30 ± 1.28	-

*Data represent mean ± SD of at least triplicate measurements. **Significant difference between incubation conditions by paired t-test ($p \leq 0.01$)*

Table 3

Summary of pharmacokinetic estimates of pitavastatin and rosuvastatin in the presence of single ascending doses of rifampicin in cynomolgus monkey

	Control	+Rifampicin 1mg/kg	+Rifampicin 3mg/kg	+Rifampicin 10mg/kg	+Rifampicin 30mg/kg
	Mean ± SD	Mean ± SD	Mean ± SD	Mean ± SD	Mean ± SD
Pitavastatin					
CL (mL/min/kg)	18.0 ± 4.6	15.0 ± 2.5	7.5 ± 2.0	4.9 ± 1.3	4.3 ± 1.6
Fold change		*0.83*	*0.42***	*0.27***	*0.24***
Vd_{ss} (L/kg)	1.79 ± 0.72	1.97 ± 0.50	0.47 ± 0.20	0.52 ± 0.16	0.55 ± 0.20
Fold change		*1.10*	*0.26***	*0.29***	*0.30***
$t_{1/2}$ (h)	5.9 ± 0.9	7.2 ± 1.7	2.9 ± 1.9	3.8 ± 0.7	4.5 ± 0.6
Fold change		*1.21*	*0.50***	*0.63*	*0.76*
Oral AUC_{last} (ng.h/mL)	299 ± 146	515 ± 417	2690 ± 2710	4070 ± 4357	5808 ± 4579
Fold change		*1.72*	*8.99***	*13.60***	*19.41***
Oral C_{max} (ng/mL)	225 ± 200	520 ± 822	2730 ± 2040	1920 ± 2950	2780 ± 3166
Fold change		*2.31*	*12.13***	*8.53***	*12.36***
Rosuvastatin					
CL (mL/min/kg)	27.5 ± 7.8	23.6 ± 2.4	20.0 ± 2.1	15.6 ± 1.9	13.4 ± 3.7
Fold change		*0.86*	*0.73*	*0.57***	*0.49***
Vd_{ss} (L/kg)	0.67 ± 0.41	0.61 ± 0.06	0.64 ± 0.16	0.71 ± 0.08	0.79 ± 0.16
Fold change		*0.91*	*0.96*	*1.05*	*1.17*
$t_{1/2}$ (h)	2.5 ± 0.7	2.5 ± 0.8	2.1 ± 0.3	3.1 ± 0.1	4.8 ± 2.0
Fold change		*1.01*	*0.86*	*1.23*	*1.93**
Oral AUC_{last} (ng.h/mL)	49 ± 12	63 ± 28	232 ± 43	467 ± 267	744 ± 512

Fold change		*1.28*	*4.68***	*9.41***	*15.01***
Oral C_{max} (ng/mL)	15 ± 11	24 ± 29	122 ± 46	150 ± 100	227 ± 169
Fold change		*1.54*	*7.72***	*9.49***	*14.37***
Rifampicin					
Oral AUC_{last} (ng.h/mL)		985 ± 396	11300 ± 3260	70100 ± 10800	240000 ± 73900
Dose-normalized change related to 1mg/kg		-	*3.8*	*7.1*	*8.1*
Oral C_{max} (ng/mL)		176 ± 99	2050 ± 245	7980 ± 2480	24200 ± 14100
Dose-normalized change related to 1 mg/kg		-	*3.8*	*4.5*	*4.6*

*Data represent mean and standard deviation (N=4). One-way ANOVA with Dunnett's multiple comparisons test was employed to test significance with *p<0.05 and **p<0.01.*

JPET Fast Forward. Published on April 11, 2018 as DOI: 10.1124/jpet.118.247767
This article has not been copyedited and formatted. The final version may differ from this version.

Figure 1

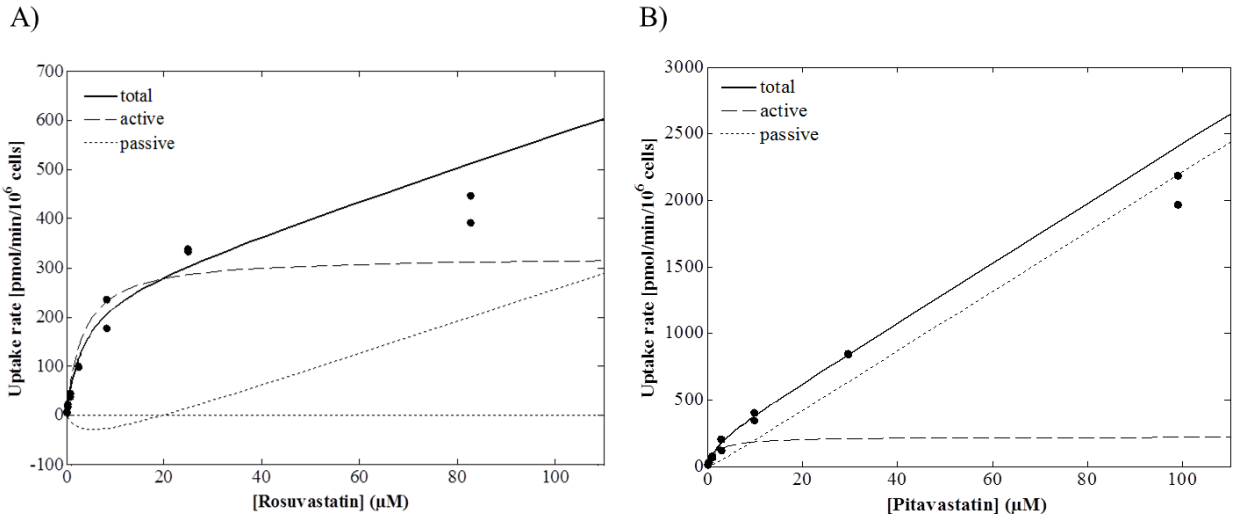

JPET Fast Forward. Published on April 11, 2018 as DOI: 10.1124/jpet.118.247767
This article has not been copyedited and formatted. The final version may differ from this version.

Figure 2

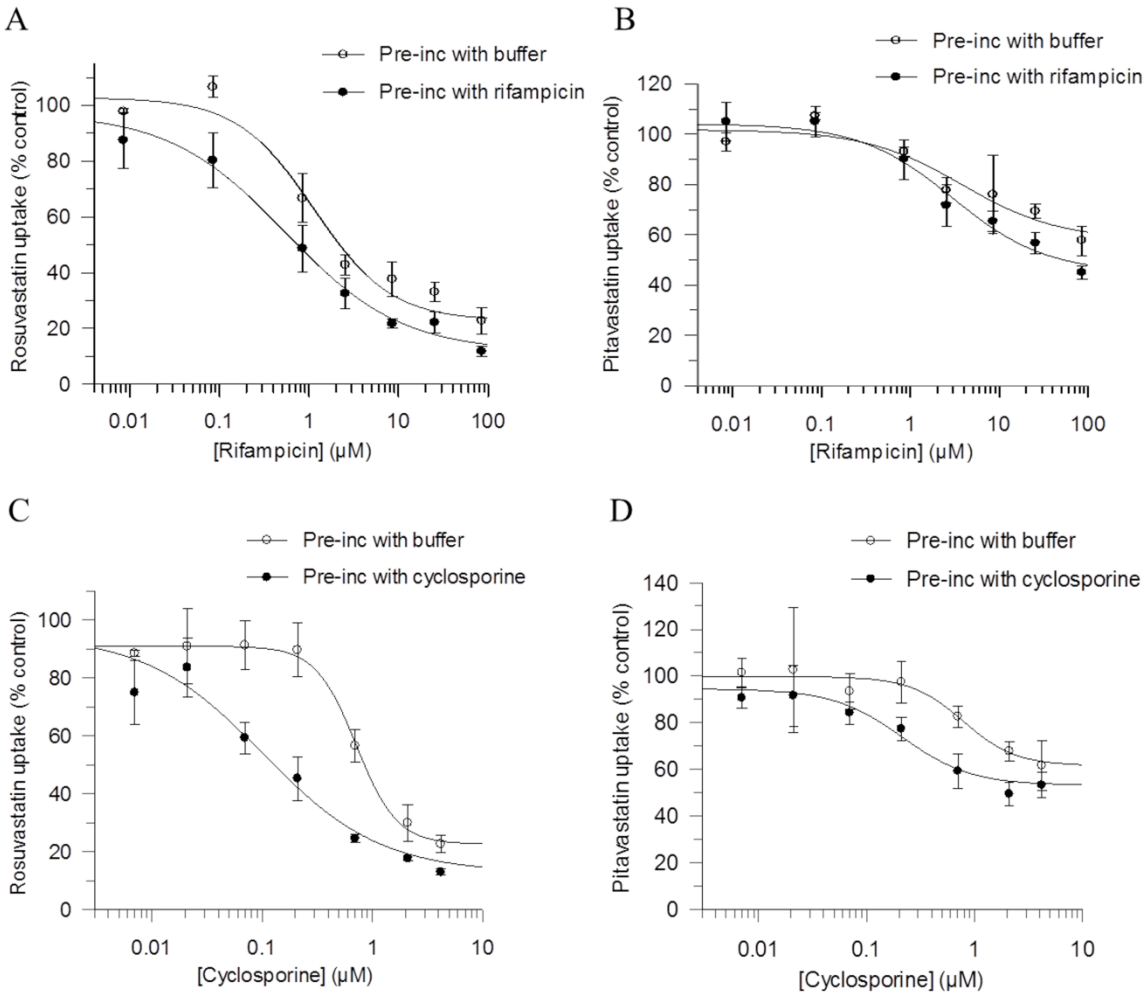

JPET Fast Forward. Published on April 11, 2018 as DOI: 10.1124/jpet.118.247767
This article has not been copyedited and formatted. The final version may differ from this version.

Figure 3

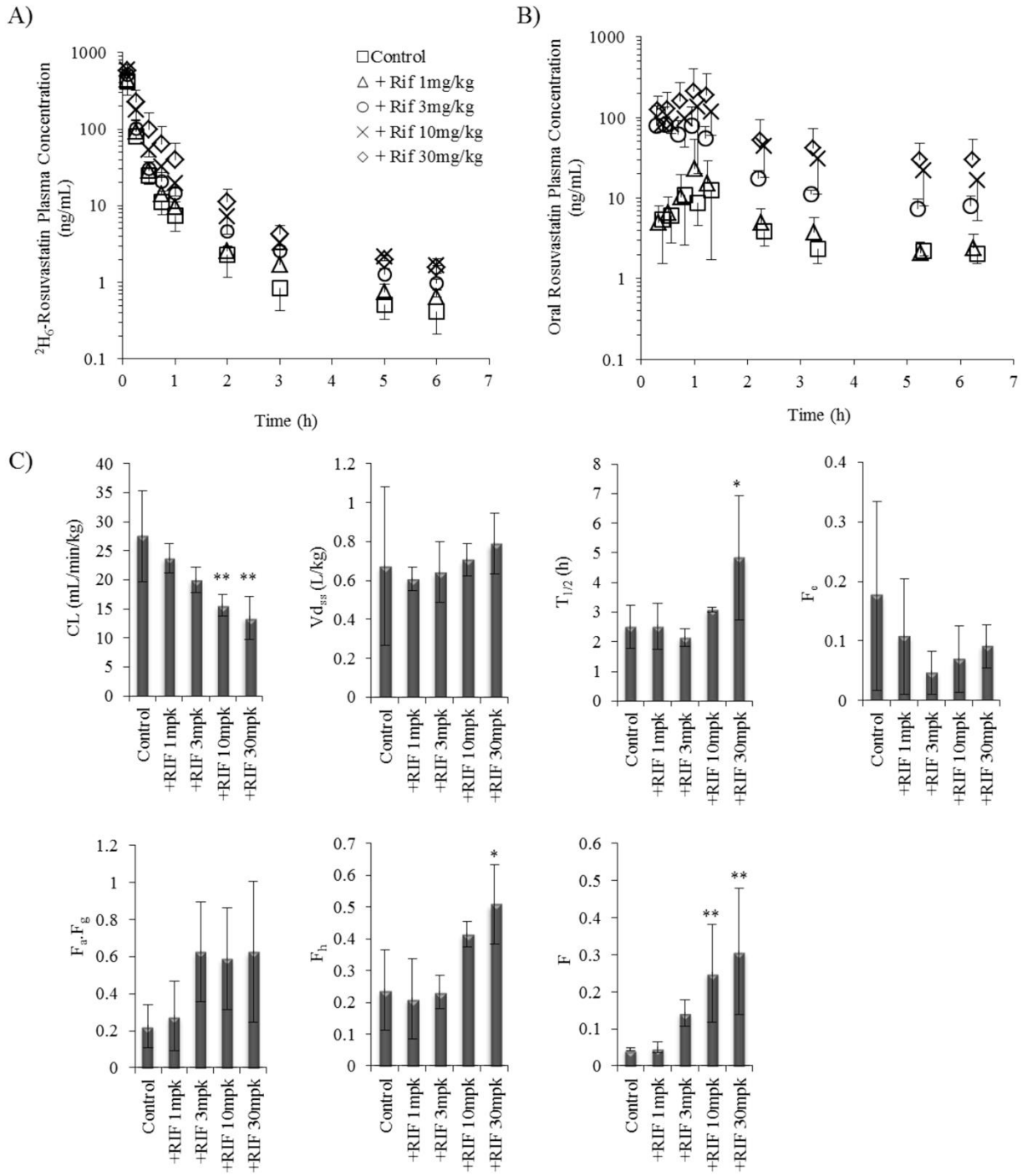

JPET Fast Forward. Published on April 11, 2018 as DOI: 10.1124/jpet.118.247767
This article has not been copyedited and formatted. The final version may differ from this version.

Figure 4

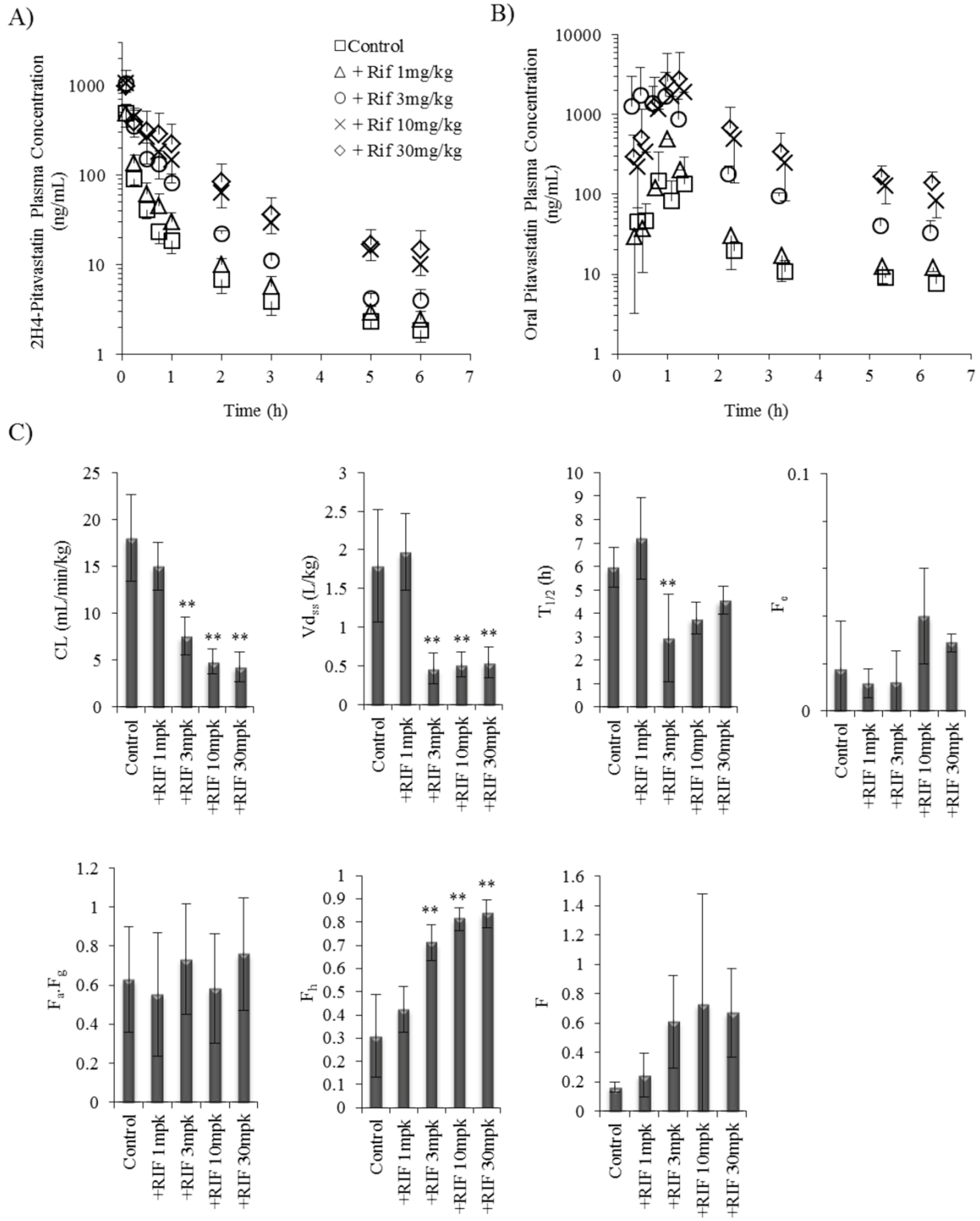

JPET Fast Forward. Published on April 11, 2018 as DOI: 10.1124/jpet.118.247767
This article has not been copyedited and formatted. The final version may differ from this version.

Figure 5

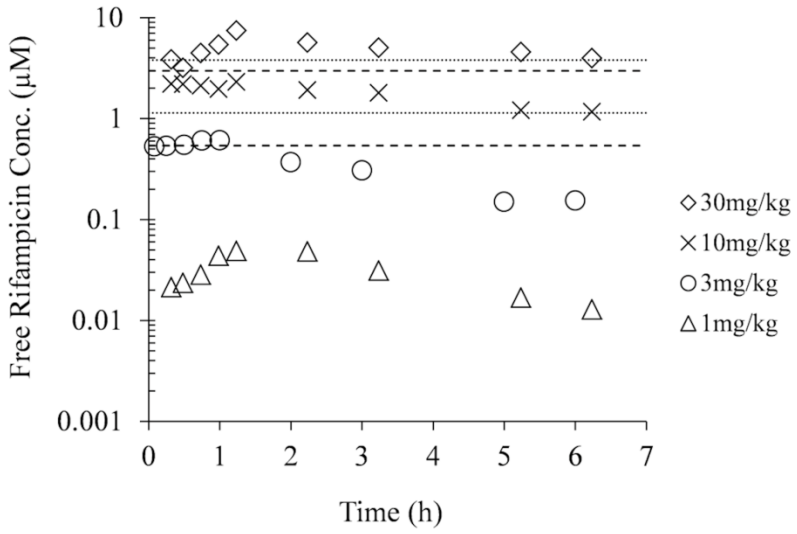

JPET Fast Forward. Published on April 11, 2018 as DOI: 10.1124/jpet.118.247767
This article has not been copyedited and formatted. The final version may differ from this version.

Figure 6

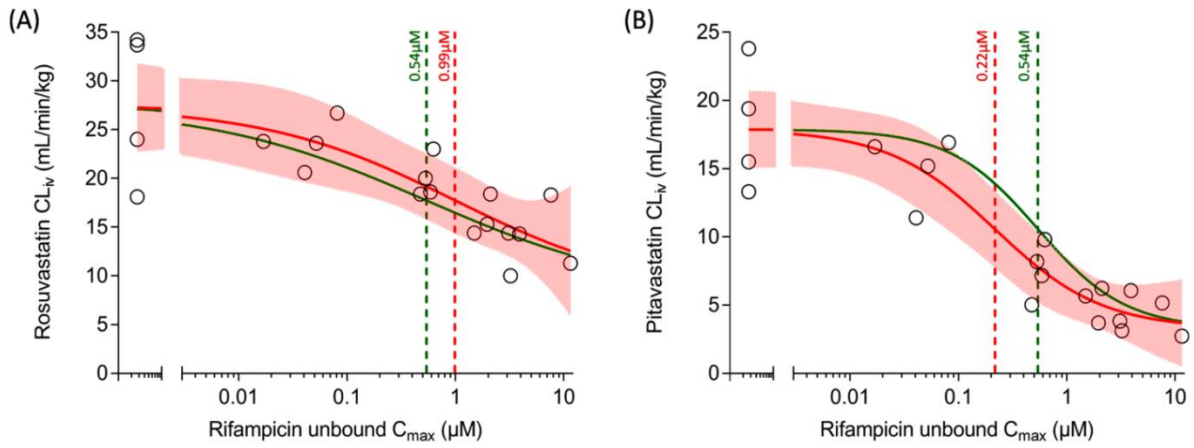

JPET Fast Forward. Published on April 11, 2018 as DOI: 10.1124/jpet.118.247767
This article has not been copyedited and formatted. The final version may differ from this version.

Figure 7